Whole genome mutational analysis for accurate tumor-informed ctDNA based MRD surveillance, treatment monitoring and biological characterization of urothelial carcinoma

Iver Nordentoft[1,*], Sia Viborg Lindskrog[1,2,*], Karin Birkenkamp-Demtröder[1,2], Santiago Gonzalez[3], Maja Kuzman[3], Jurica Levatic[3], Dunja Glavas[3] , Ryan Ptashkin[3], James Smadbeck[3], Danielle Afterman[4], Tomer Lauterman[4], Yarin Cohen[4], Zohar Donenhirsh[4], Iman Tavassoly[3], Ury Alon[4], Amanda Frydendahl Boll Johansen[1,2], Mads Heilskov Rasmussen[1,2], Claus Lindbjerg Andersen[1,2], Paz Polak[3], Asaf Zviran[3], Boris Oklander[4], Mads Agerbæk[5], Jørgen Bjerggaard Jensen[2,6], Lars Dyrskjøt[1,2]

[1]Department of Molecular Medicine, Aarhus University Hospital, Aarhus, Denmark

[2]Department of Clinical Medicine, Aarhus University, Aarhus, Denmark

[3]C2i Genomics. INC, New York, NY, USA

[4]C2i Genomics. LTD, Haifa, Israel

[5]Department of Oncology, Aarhus University Hospital, Aarhus, Denmark

[6]Department of Urology, Aarhus University Hospital, Aarhus, Denmark

* authors contributed equally

Abstract

Circulating tumor (ctDNA) can be used for sensitive detection of minimal residual disease (MRD). However, the probability of detecting ctDNA at low tumor burden is limited by the number of mutations analyzed and available plasma volume. Here we applied a tumor-informed WGS approach for ctDNA-based MRD detection (91% sensitivity, 92% specificity) and treatment response evaluation in 916 longitudinally collected plasma samples from 112 patients with localized muscle-invasive bladder cancer. We show that WGS-based ctDNA detection is prognostic of patient outcomes with a median lead time of 131 days over radiographic imaging. We performed genomic characterization of post-treatment plasma samples to study tumor evolution and observed acquisition of the platinum therapy-associated mutational signatures and copy number variations not present in the primary tumors. Our results support the use of WGS for ultra-sensitive ctDNA detection, and highlight how tracking of tumor evolution using WGS of plasma samples opens opportunities to refine precision oncology.

Introduction

Tumor cells release cell-free DNA (cfDNA) with tumor specific molecular alterations into circulation (circulating tumor DNA; ctDNA) mainly by cell death[1]. ctDNA is cleared from circulation through nuclease digestion, renal clearance, or uptake by the liver and spleen[2–5]. Furthermore, the ctDNA half-life is between 15 min and 2 hours[6], making it possible to use ctDNA for tracking of tumor burden following surgery and through oncological treatment. Recent studies have shown that ctDNA is a powerful biomarker for detection of minimal residual disease (MRD) and relapse in multiple cancer types[7,8] - including bladder cancer (BC)[9]. Globally, more than 570,000 patients are diagnosed with BC each year[10]. Curative intended radical cystectomy (RC) preceded by neoadjuvant chemotherapy (NAC) is the standard of care for localized muscle-invasive bladder cancer (MIBC). However, nearly half of patients will experience metastatic relapse mainly within the first 2 years after surgery, when considering all stages[11]. Therefore, reliable diagnostic and prognostic biomarkers with high sensitivity and specificity are needed to improve detection of MRD for earlier initiation of oncological treatment and potentially improve patient outcomes. Previous ctDNA studies in patients with BC have demonstrated that ctDNA can be detected on average 3 months prior to metastatic relapse detected by radiographic imaging[9]. In addition, ctDNA has been correlated to chemo- and immunotherapy response[9,12,13]. The low tumor fraction typically observed post surgery limits the probability of detecting ctDNA-based MRD. Tumor-informed ctDNA detection approaches have the highest sensitivity and specificity, however, it is also usually more labor intensive compared to non-tumor informed detection methods. Furthermore, the probability of detecting ctDNA is limited by the number of mutations analyzed, the available plasma volume and the depth of sequencing[14]. Recent studies have demonstrated the feasibility of WGS-based analysis and the joint utilization of mutations and copy number alterations allows for ultra-sensitive ctDNA detection[15,16]. In addition, WGS-based analysis of ctDNA also facilitates characterization of tumor biology in a metastatic setting enabling tracking of tumor evolution including identification of acquired treatment targets during surveillance and oncological treatment[17].

Here we implemented and applied a WGS approach to monitor ctDNA for sensitive MRD detection and treatment response prediction in 112 patients with localized MIBC. Furthermore, we analyzed genome-wide alterations in tumor and plasma samples to investigate tumor evolution and treatment resistance.

Results

Patient characteristics and WGS data generation

A total of 112 patients with localized MIBC treated with NAC before RC were prospectively enrolled for liquid biopsy analysis between 2014 and 2021 at Aarhus University Hospital, Denmark (**Extended Data Table 1**). Plasma samples for ctDNA analysis were procured before, during and after NAC, and at scheduled control visits after RC (n = 916; **Fig. 1a**). 110 of the patients underwent RC with a median follow-up time of 53.6 months after RC. We observed a recurrence rate of 24% (26/110), pathological downstaging to a non-invasive stage (≤pTa,CIS,N0) for 61% (67/110) and complete pathologic response (pCR, pT0/pTIS) for 58% (64/110). WGS of tumor- and matched PBMC DNA was performed at a mean genome coverage of 59 and 33 for formalin fixed paraffin embedded (FFPE) and tumor fresh frozen samples, respectively, and 31 for PBMC DNA. WGS of cfDNA from plasma (n=916) was performed at a mean genome coverage of 28.

ctDNA detection by tumor-informed WGS models

For ctDNA detection we developed patient-specific, tumor-informed WGS models by integrating genome-wide somatic alteration patterns coupled with advanced signal processing and AI-based error suppression (see materials and methods; **Fig. 1b**). These patient-specific models were applied to WGS data from plasma cfDNA. For initial validation of the robustness of the WGS ctDNA analysis pipeline, we compared ctDNA calls by analyzing technical replicates (tumor-, PBMC- and plasma DNA) performed independently in two different laboratories (USA, DK) using similar protocols (**Fig. 1c**) including 166 plasma samples from 18 patients. Of these, 52 samples had a tumor fraction above the detection threshold in one or both laboratory sites. A high correlation of estimated tumor fractions between laboratory sites was observed, with the coefficient of determination being R^2=0.8 including all samples and R^2=0.99 restricting to samples detected positive in both laboratory sites (red circles, **Fig. 1c**).

WGS-based ctDNA detection for prognosis and metastatic relapse

The prognostic value of ctDNA was investigated using the 916 plasma samples collected during the disease courses of the 112 patients: i) at diagnosis prior to NAC (preNAC), ii) after NAC and before RC (preRC) and iii) during disease surveillance after RC (postRC; **Fig. 2, Extended Data Fig. 1**). Detection of ctDNA was highly prognostic of patient outcomes: at diagnosis before NAC (Recurrence-free survival [RFS]: HR=7.7, 95%CI=2.3-26.3, *p*=0.0001; overall survival [OS]: HR=9.2, 95%CI=2.7-31.5, *p*=0.0001), at preRC (RFS: HR=3.4, 95%CI=1.5-7.8, *p*=0.0018; OS: HR=4, 95%CI=1.8-8.8, *p*=0.0003), and after RC (accumulated

ctDNA status up to 1 year after RC; RFS: HR=21.5, 95%CI=7.4-62.6, *p*<0.0001; OS: HR=29.1, 95%CI=9.9-85.7, *p*<0.0001; RFS: **Fig. 3b,e,h**; OS: **Fig. 3c,f,i**).

The presence of ctDNA after RC reflecting MRD showed the highest correlation to outcome. Using accumulated ctDNA status up to one year after cystectomy and relapse within 18 months of the last plasma sample, resulted in a sensitivity of 91% and a specificity of 92% (**Fig. 3g**). Using the same criteria, pathological downstaging predicted metastatic relapse with a sensitivity of 83% and specificity of 77% (Data not shown). In 70% of patients with metastatic relapse (18/26), ctDNA was detected before clinical recurrence (radiographic imaging positive; **Fig 2**). Overall, the median lead time of ctDNA detection was 131 days (−106 to 1156, p<0.00001) over radiographic imaging for patients with detectable ctDNA after RC (full follow-up included; **Fig 4a**).

ctDNA detection for evaluation of treatment response

ctDNA status preNAC and preRC was significantly associated with pathological downstaging (*p*=0.00001, *p*=0.018, **Fig. 4b,c**) and pCR (*p*=0.00001, *p*=0.038, data not shown). The ctDNA dynamics during NAC (ctDNA either remained detectable, was cleared during NAC or persisted ctDNA negative) was also a predictor of pathological downstaging (p<0.00001, **Fig. 4d**). Pathological downstaging was *per se* a strong predictor of metastatic relapse with a recurrence rate of 2% (1/54) for downstaging and 40% (12/30) for non-downstaging patients (**Fig. 4e,f)**. While the pathological evaluation of NAC response uses local tumor response as a proxy of systemic response, ctDNA status preRC provides a measurement for local response and metastatic burden. Thus, we investigated ctDNA as a treatment response parameter for distant micrometastatic disease. The analysis was restricted to patients receiving a minimum of 3 NAC cycles to ensure adequate treatment (**Fig. 4g**). Patients remaining ctDNA negative throughout NAC (all negative, n=38) had a very favorable outcome with only one patient experiencing metastatic recurrence. For patients with ctDNA clearance during NAC, 19% (5/26) of patients recurred. Finally, patients who remained ctDNA positive during NAC, had an unfavorable outcome with a recurrence rate of 55% (5/9). Plasma ctDNA dynamics was furthermore strongly associated with RFS with particularly poor outcome for patients where ctDNA remained detectable (**Fig. 4h**). Alluvial plots showing ctDNA status during the disease courses are shown in **Extended Data Fig. 2**.

ctDNA detection levels of different metastatic sites

As the level of ctDNA detected after RC varied, we hypothesized that the tumor fraction could be related to the metastatic site. Interestingly, significantly lower tumor fractions were detected for patients with lung metastasis compared to all other metastatic sites (*p*=0.0087, **Fig. 4i**) as

well as compared to metastases from bone (p=0.003), kidney (p=0.002), liver (p=0.035) and pelvis (p=0.047) individually (**Fig. 4j**).

Biological characterization of primary tumors by WGS analysis

WGS analysis of the primary tumor for 112 patients revealed a median of 23,851 single-nucleotide variants (SNVs) and 674 indels per tumor. An overview of selected genomic alterations from known bladder driver genes[18] is shown in **Fig. 5a**. *TP53*, *RB1*, *KMT2D*, *ARID1A* and *KDM6A* were the most frequently mutated genes and 55% of tumors had a *TERT* promoter mutation (**Fig. 5a**). In total, 16 significantly mutated genes were identified using dndscv[19], an algorithm based on the dN/dS ratio while correcting for trinucleotide mutation rates to look for signals of positive selection to identify cancer driver genes (**Extended Data Table 2**). Among the most significantly mutated genes, dndscv identified *TP53*, *RB1*, *KDM6A* and *ARID1A*, confirming a good correlation between both approaches (highlighted with asterisks in **Fig. 5a**). Whole-genome doubling (WGD) was identified in 51% of tumors (57/112) by separating tumors based on ploidy and the level of heterozygosity[20,21](**Extended Data Fig. 3a**). WGD has previously been associated with worse prognosis[22]; however, we observed no association of WGD and worse RFS or OS (**Extended Data Fig. 3b,c**).

De novo extraction of single-base substitutions (SBS) signatures revealed eight mutational signatures in the profiled tumor genomes, of which seven were decomposed to the known SBS1, SBS2, SBS5, SBS13, SBS17a, SBS17b, and SBS92. APOBEC-induced mutagenesis was identified as the primary contributor to the mutational landscape of the tumors with median 42% of SNVs per patient being attributed to SBS2 or SBS13 mutational contexts (**Fig. 5a**). The SBS92 signature was first identified in normal bladder tissue of smokers[23] and has subsequently been attributed to tobacco smoking mutagenesis in BC using the PCAWG dataset[24]. Here, 45 tumors had SBS92-related mutations and we observed a significantly higher number of SBS92-related mutations in tumors from current smokers compared to tumors from former- and never smokers (p<0.0001; **Fig. 5b**). For current or former cigarette smokers, the number of mutations in the SBS92 context was not associated with the number of cigarette pack years (**Fig. 5c**). The SBS92 signature was also detected in plasma samples collected after RC for three patients with metastatic relapse (**Fig. 6a**). *De novo* extraction of small insertion-and-deletion (ID) signatures revealed 10 signatures of which seven were decomposed to the ID signatures previously observed in BC[25] (ID1, ID2, ID3, ID4, ID5, ID8, ID9) and the remaining to the known ID14, ID15 and ID16 (**Fig. 5a**). ID1, ID3 and ID8 were identified as the primary contributors, each accounting for >15% of all observed indels. The ID3 signature has previously been associated with tobacco smoking[25]. Here, 66 tumors had ID3-related indels and we observed a significantly higher number of ID3-related indels in

tumors from current smokers compared to tumors from former- and never smokers (p=0.0004; **Fig. 5d**). Again, the number of indels in the ID3 context was not associated with the number of cigarette pack years (**Fig. 5e**). For current smokers, 90% (44/49) showed either SBS92- or ID3-related alterations and 51% (25/49) showed contribution from both signatures (**Extended Data Fig. 3d**). In comparison, only 28% (5/18) of never smokers showed contribution from either SBS92 or ID3, highlighting the divergent mutational landscape of tumors from smoking and non-smoking patients. No association between smoking status and number of SNVs or indels was observed (**Extended Data Fig. 3e,f**).

Of interest, patient 5350 displayed a novel SBS signature characterized by T>A and T>C mutations (**Extended Data Fig. 4a**; referred to as SBSX), which was not present in the existing databases[26,27] and could not be reconstructed by known signatures. The same mutations contributing to this context were identified in a plasma sample taken 379 days after RC as well, thus confirming the presence of the signature (**Extended Data Fig. 4b,c**). The tumor from patient 5350 is among the most mutated in the cohort (98,036 SNVs) and the novel signature contributed to 80% of the total mutational burden (**Fig. 5a**). A deeper inspection of its activity showed a strong transcriptional strand bias and enrichment in intergenic regions (**Extended Data Fig. 4d**). Similar patterns are observed for transcription coupled nucleotide excision repair (TC-NER) processes that are involved in UV and tobacco damage repair and may indicate that TC-NER is associated with this signature[28,29]. It is noteworthy that patient 5350 was diagnosed with a primary neuroendocrine carcinoma accounting for <1% of all BC cases being an aggressive tumor associated with poor prognosis, and was treated for esophageal cancer seven years before the bladder tumor.

We compared genomic variables to chemotherapy response evaluations. We found no significant association between response to NAC and number of SNVs, indels or WGD (**Extended Data Fig. 3g-i**). As previously observed[30], we confirmed a significant association between SBS5 contribution and *ERCC2* mutations (p<0.0001; **Extended Data Fig. 3j**). Although neither the level of SBS5-related mutations nor *ERCC2* mutations were independently associated with response to NAC (**Extended Data Fig. 3k,l)**, combining *ERCC2* mutations and the level of SBS5-related mutations showed that 77% of patients with an *ERCC2* mutation and/or high SBS5 contribution (above median) showed pathological downstaging after NAC, whereas patients with *ERCC2* wildtype and/or low SBS5 contribution had a response rate of 56% (p=0.026; **Fig. 5f**).

Tumor evolution resolved from WGS-based ctDNA analysis

WGS of cfDNA from plasma samples with high tumor fraction allows for characterization of tumor evolution[31,32]. In 38% of patients with metastatic relapse (10/26), the detected cfDNA tumor fraction was sufficient (>10%) to perform a post-treatment genomic characterization independently of their initial tumor biopsy. In total, we performed *de novo* somatic calling of variants for 15 plasma samples from those 10 patients.

Six plasma samples from four patients (5408, 5113, 4119 and 4105; 40% of included plasma samples) showed contribution of the platinum therapy-associated mutational signatures SBS31 or SBS35 (**Fig. 6a,b**). Importantly, the two chemotherapy-induced mutational signatures were not observed in any of the primary tumors and were only observed when analyzing plasma-specific mutations. For all four patients, the SBS31/35 signatures were observed in plasma samples collected 239-571 days after initiation of NAC (plasma samples collected earlier in the disease course of the patients were not characterized due to too low tumor fraction). None of the four patients had a pathological response to NAC; however, the presence of chemotherapy-induced mutational signatures in the plasma samples may indicate clonal expansions after the gemcitabine/cisplatin treatment.

The driver mutations identified in primary tumors remained mostly identical to the mutations observed in post-treatment plasma samples. New driver mutations were only detected for patient 5350 where predicted driver mutations in *ASXL2* and *NFE2L2* were observed in the plasma sample collected 379 days after RC. *ASXL2* is involved in chromatin remodeling and *NFE2L2* is a transcription factor involved in the regulation of oxidative stress and inflammatory responses and mutations in these genes have previously been observed in BC[33,34].

Remarkably, we observed an evolution of the CNVs detected in post-treatment plasma samples compared to the primary tumor for all 10 patients, suggesting that the clone overcoming treatment differs from the sequenced part of the primary tumor (**Fig. 6c**). In the two analyzed plasma samples collected after RC for patient 4105 (one of the patients having chemotherapy-induced mutational signatures), we observed a focal amplification on chromosome 4 affecting the primary tumor driver variant *FGFR3* p.S249C, and an increase in copy number on chromosomes 19q and 20 not detected in the primary tumor (**Fig. 6d**). In the plasma sample collected during NAC for patient 5408, newly acquired copy number gains on chromosomes 17, 19p and 22 were observed (**Extended Data Fig. 5**). Opposite to those large genomic changes, the three plasma samples collected after RC for patient 5113 were all highly representative of the primary tumor without minor recurrent acquired variations, indicating limited evolution after treatment (**Fig. 6d**).

Discussion

We applied a WGS approach to monitor ctDNA for MRD detection in patients with localized MIBC, and documented the prognostic role of ctDNA at diagnosis, before RC and during surveillance. Our findings underline a role for ctDNA in guiding treatment decisions in BC in line with previous findings from other patient cohorts[9,12,13,35,36]. An important aspect of this WGS approach is its high sensitivity and specificity, which is comparable to other established tumor-informed tests applied in this setting, matched the ease of performing WGS without any need for designing personalized assays. ctDNA analysis using WGS may drive the field forward faster and facilitate a rapid generation of test results to establish clinical utility thus paving the way for novel trial designs. Prospective ctDNA WGS analysis for MRD detection seems very promising with low false negative rates, and may soon be implemented for informed selection of patients for adjuvant treatments. In line with this, ongoing clinical trials will demonstrate if early ctDNA-guided treatment in the adjuvant setting is beneficial compared to treatment initiation upon detection of metastatic relapse based on radiographic imaging[37,38]. In addition, this study also supports the rationale behind investigating the benefit of NAC administration for ctDNA negative patients, and whether bladder sparing approaches can be applied based on ctDNA testing.

We identified significantly lower tumor fractions for patients with lung metastasis compared to other metastatic sites, indicating a correlation between extent of detectable ctDNA and location of metastasis. These findings are in accordance with a recent study on metastatic colorectal cancer showing that patients with lung-only and peritoneum-only metastatic disease had significantly lower levels of ctDNA compared to other metastatic sites[39], indicating a decreased detection sensitivity. Early detection of MRD using WGS approaches may result in improved detection in BC patients with lung metastasis.

When exploring mutational signatures present in primary tumor biopsies, we identified the contribution of SBS92 to be associated with the smoking status of patients as previously observed in malignant and non-malignant bladder tissue[23,24]. SBS92 was recently identified in non-small cell lung cancer using deep WES (median of 413x)[40]; however, SBS92 has not previously been identified in exome-sequenced bladder tumors as the signature is mostly located in intergenic regions[24]. This highlights the importance of using WGS data to unravel the full genomic landscape of BC genomes. Patient 5350 displayed a novel signature, SBSX, which could not be reconstructed by known public databases of signatures. Although the signature was only observed in a single patient, we found the same signature in a post-treatment plasma sample as well, thus confirming that the signature is related to biology rather than being technically introduced. The identification of a novel signature contributing to 80%

of the total mutational burden for patient 5330 claims the need for an exploration of whether the signature is present in larger patient cohorts.

Our WGS strategy for ctDNA-based MRD detection allows for direct genomic characterization of plasma cfDNA independently of the initial tumor biopsy. This approach holds huge potential for increasing our understanding of tumor evolution and treatment resistance mechanisms. First, metastatic tumor biology can be fully unraveled. It has been shown that ctDNA contains multiple subclones and that synchronous metastatic tissue biopsies only comprise a small fraction of the total ctDNA[17]. Analysis of plasma samples can thereby overcome tissue sampling bias leading to clonal illusion and underestimated heterogeneity to recapitulate the complete metastatic disease burden of the patients[41]. Second, tumor evolution and therapy-induced shifts in selection pressure can be longitudinally tracked. Tumor biology evolves over time and during treatment pressure, underlining the importance of having a real-time snapshot of the current tumor biology when making treatment decisions in the metastatic setting. Analysis of plasma samples during and after treatment could thereby serve as a minimally-invasive measure of treatment response (ctDNA clearance) and provide additional information of possible oncological treatment options.

Here, we observed a contribution of the platinum therapy-associated mutational signatures SBS31 or SBS35 in six post-treatment plasma samples from four patients, indicating cisplatin mutagenesis and clonal expansions after NAC. Furthermore, in the post-treatment plasma samples for patient 4105, we observed an acquired focal amplification of the *FGFR3* gene on chromosome 4, indicating that Erdafitinib, a pan-FGFR inhibitor approved as second-line treatment for patients with advanced BC[42], could be a potential treatment option for this patient. These observations highlight how post-treatment tumor characterization using cfDNA provides information on the genomic changes acquired since the initial tumor biopsy, which could improve identification of therapeutic targets and provide information on possible treatment resistance at an early time point. A previous study performed deep WGS of plasma samples with high ctDNA fractions (17-82%) from patients with metastatic prostate cancer which, amongst several findings, revealed treatment-driven selection for androgen receptor augmentation[17]. Overall, the study highlighted how deep WGS of plasma samples is a superior approach to achieve high resolution of treatment-associated dynamics and resistance mechanisms compared to analyzing metastatic tissue biopsies. To build on our findings presented here, WGS analysis of metastatic tissue biopsies could be performed to study whether ctDNA comprises additional subclones and intra-patient heterogeneity not present in a single metastatic tissue biopsy. Furthermore, the sequencing depth of plasma samples with high ctDNA fractions could be increased to study clinically actionable gene mutations and treatment resistance mechanisms further. The sequencing depth of 20x is a limitation for

studying individual sites, and acquisition of new driver mutations was only observed for patient 5350 (tumor fraction of 50%) in our current analysis of mutational driver events in post-treatment plasma samples. Increasing the sequencing depth may also allow for biological characterization of plasma samples with a tumor fraction below the currently applied cut-off of 10%.

Our study highlights that WGS-based analysis of cfDNA allows ultra-sensitive ctDNA detection in patients with MIBC. ctDNA testing holds huge potential to change the current clinical management of patients with more individualized treatment and tracking of tumor evolution using WGS of cfDNA opens opportunities to refine precision oncology.

Materials and methods

Patients and clinical follow-up

In total, 112 patients diagnosed with MIBC treated with NAC and RC were enrolled between 2013 and 2021 at Aarhus University Hospital in Denmark. Detailed follow-up data were available for all patients with a median follow-up of 1841 days after RC (range: 139-2810) for patients without clinical relapse. Recurrence data were obtained from computed tomography scans (CT-scans, PET/CT scans) or pathology reports and survival data were obtained from the nationwide civil registry. pCR to NAC was defined as pT0/pTIS/N0 and non-invasive downstaging after NAC was defined as pT0/pTIS/Ta/N0. All patients provided informed written consent, and the study was approved by The National Committee on Health Research Ethics (#1302183). Study data were collected and managed using REDCap hosted at Aarhus University[43,44].

Biological samples

Tumor samples were procured from transurethral resection of the bladder (TURBT) at the time of diagnosis (n=112). DNA was extracted from sections of Tissue-Tek O.C.T Compound embedded tissue or punches of formalin-fixed paraffin embedded tissue (FFPE) using Puregene DNA purification kit (Gentra Systems). Leukocyte DNA was extracted from the buffy coat from all patients using the QIAsymphony DSP DNA midi kit (QIAGEN). Cell-free DNA (cfDNA) was extracted from 2 mL of plasma using QIAamp Circulating Nucleic Acid Kit (QIAGEN, Hilden, Germany) and eluated in 60 µL buffer EB (QIAGEN). Blood samples were collected at scheduled clinical visits. The cfDNA percentile was estimated from TapeStation 4200 (Agilent) by size window: (100bp – 500bp) using the Cell-free DNA ScreenTape assay. High molecular fragments >500bp as a measure of genomic DNA contamination served as exclusion criteria if >30%. Total cfDNA concentration was measured using ddPCR assays for

2 stable regions on chromosome 16 and chromosome 3[45]. Automated Droplet Generator (Bio-Rad) were used for Droplet generation, and readout was performed on a QX200™ Droplet Reader (Bio-Rad).

Whole Genome Sequencing

Libraries of tumor and matching germline DNA were prepared using the Twist Library preparation EF kit (Twist Bioscience) with an input of 200 ng DNA. The protocol utilizes enzymatic fragmentation; however, the fragmentation time was decreased to 6 minutes for the FFPE samples to account for degraded DNA. For buffy coat DNA and DNA from fresh frozen tumors, a 10 minutes fragmentation time was used. The protocol was optimized using the xGEN™ UDI-UMI Adapters (Integrated DNA Technologies) with 7 cycles of PCR post ligation. The UMI part was not sequenced as UMI correction is only beneficial for deep sequencing. Libraries of cfDNA from plasma were prepared using the KAPA HyperPrep kit (Roche) with the xGEN™ UDI-UMI Adapters (Integrated DNA Technologies) using cfDNA input equal to 1-2 mL of plasma and 7 cycles of PCR post ligation. A minimum input of 5 ng was used. All libraries were paired-end sequenced (2x150 bp) on the NovaSeq 6000 platform (illumina) using S4 flow cells. Prior to sequencing all runs were calibrated on a MiSeq Nano (2x150 bp) to obtain even coverage.

Preprocessing of WGS data and quality control analysis

WGS reads for primary tumors, matched germline and plasma samples were demultiplexed using Illumina's bcl2fastq to generate FASTQ files. The genetic concordance of FASTQ files from the same patient was confirmed using NGSCheckMate[46]. FASTQ files from all three sample types were trimmed with Skewer v0.2.2[47] to remove paired-end adapter sequences. Both the untrimmed and trimmed FASTQ files were run through FastQC v0.11.9 to identify potential problems in sequencing. The trimmed FASTQ files were aligned to the reference genome (GRCh38) with BWA MEM v 0.7.17. The resulting aligned bam files were sorted with Samtools v1.14.

Each per-lane BAM file was marked for duplicate reads using GATK[48] MarkDuplicatesSpark v.4.1.8.0 resulting in a duplicate-marked BAM that was passed for calculation and recalibration of the per-read base quality score using GATK BQSRPipelineSpark. Each recalibrated BAM file was indexed and re-sorted by read name using Samtools v1.11. GATK MarkDuplicatesSpark was used to merge all BAM files from the same sample. This process produced the final coordinate sorted BAM file for each sample.

Alignment quality control metrics were computed on the BAM file using Picard (QualityScoreDistribution, MeanQualityByCycle, CollectBaseDistributionByCycle,

CollectAlignmentSummaryMetrics, CollectInsertSizeMetrics, CollectGcBiasMetrics, CollectOxoGMetrics) and GATK (average coverage, percentage of mapped and duplicate reads). These metrics were used to identify potential problems in sequencing or preprocessing.

Tumor/normal somatic mutation calling

Each tumor and matched germline BAM files were analyzed using GATK Mutect2 v4.2.4.1 and Strelka v2.9.10[49] to identify putative somatic single nucleotide variants (SNVs). These SNVs were filtered using GATK FilterMutectCalls to retain PASS variants and remove variants corresponding to known single nucleotide polymorphism sites (dbSNP v138), as annotated by GATK VariantAnnotator. Only SNVs detected by both Mutect2 and Stelka were retained. Finally, a panel of sequenced donor plasma samples was used to remove artifactual SNV calls from the final SNV vcf file.

Somatic INDELs were called by SVaba v1.1.3 and Mutect2 and the final list of INDELs comprised those detected by both methods. In cases where INDELs overlapped with a non-exact match, the largest INDEL was selected.

Copy number variations (CNVs) in solid tumors were called using FACETS v0.6.2[50]. Base coverage and variant allele fraction (VAF) of heterozygous SNP positions of the tumor sample and paired germline sample were used as input to the method. The list of germline heterozygous SNP positions was calculated using BCFTools mpileup[51] and a reference set of SNPs from the HapMap Project v3.3[52]. The output was processed to revert all subclonal CNV calls to the nearest clonal CNV call.

Estimation of tumor fraction in solid tumor and cfDNA

Tumor fraction estimations in both solid tumor samples and plasma samples were estimated using the in-house method C2inform which constitutes the latest version of our previous described method[15]. C2inform uses the complete set of somatic mutations found in the solid tumor to generate a patient-specific tumor signature which is used, in combination with plasma heterozygous positions, to detect the tumor presence in cfDNA and estimate its tumor fraction.

Biological characterization of tumor samples

For the purpose of tumor characterization, an in-house filtering method was applied to remove low-quality mutations with features characteristic of FFPE-induced artifacts. VEP v107.0[53] was applied to the final list of SNVs and INDELs to determine the affected gene and functional impact. We queried all non-synonymous variants of the cohort against databases of cancer

driver genes (Intogen[18] and cancer biomarkers CGI[54]) to identify the somatic mutations in genes of biological interest.

Similarly, genes affected by CNVs were classified as biologically relevant if present in a list of candidate cancer genes created by manual annotation of scientific publications[55,56].

Sigprofiler v1.1.20 was used to extract SNV and INDEL signatures in a three-step workflow: (I) De-novo extraction of signatures. (II) Fitting of selected signatures from COSMIC v3.3[25] and artifact signatures used for the detection of spurious deviations. (III) A final fitting using cancer-type exclusive signatures and the manual inclusion of select signatures determined from steps (I) and (II), that corresponds to the final set of signatures presented in the results.

Whole genome doubling (WGD) status was determined by separating each sample based on ploidy and level of heterozygosity as previously described[20,21], resulting in two separate clusters corresponding to near-diploid samples and samples with WGD.

De novo detection of somatic alterations in plasma samples with high tumor fraction

Plasma samples with a tumor fraction above 10% were selected for de-novo calling of SNVs and CNVs (See: Biological characterization of tumor samples). SNV and INDEL results from the plasma samples were compared with results from the solid tumor samples to determine shared, tumor-unique, and plasma-unique alterations.

Statistical analysis

Survival curves were compared using the Kaplan-Meier method (log rank tests). Hazard ratios (HR) and associated 95% confidence intervals (CI) were calculated using Cox regression analysis (R packages survminer v0.4.9 and survival v3.2.13). Kruskal Wallis test, Wilcoxon rank sum test, Fisher's exact test and Pearson's correlation coefficient were used to determine statistically significant associations. Analysis was performed using the R statistical environment (v4.1.2).

Data availability

The raw sequencing data generated in this study are not publicly available as this compromises patient consent and ethics regulations in Denmark. Processed non-sensitive data are available upon request from the corresponding author.

Acknowledgements

This work was funded by research grants to L.D. from C2i Genomics, The Danish Cancer Society, Novo Nordisk Foundation, Independent Research Fund Denmark, Aarhus University and Aarhus University Hospital. We would like to thank technical personnel at the Departments

of Molecular Medicine, Urology and Oncology, Aarhus University Hospital, for sample handling and processing. Sample collection was supported by the Danish Cancer Biobank.

Author contributions

L.D., A.Z., B.O., I.N. conception and design. L.D., A.Z., B.O., I.N., A.F.B.J. development of NGS methodology. I.N., A.F.B.J. NGS library generation and WGS sequencing coordination, Acquisition of data. K.B.D. selection of patients and acquisition of samples and clinical data and programming and managing of Redcap database. I.N., S.V.L., K.B.D., L.D., S.G., P.P., D.A. analysis and interpretation of data. I.N., S.V.L. S.G., P.P., L.D. wrote the manuscript, with contributions from K.B.D., M.K., J.L., D.G., R.P., J.S., D.A., T.L., Y.C., Z.D., I.T., U.A., A.F.B.J., M.H.R., C.L.A., A.Z., B.O., M.A., J.B.J.

Competing interests

Lars Dyrskjøt has sponsored research agreements with C2i Genomics, Natera, AstraZeneca, Photocure, and Ferring and has an advisory/consulting role at Ferring, MSD and UroGen. Lars Dyrskjøt has received speaker honoraria from AstraZeneca, Pfizer and Roche and received travel support from MSD. Lars Dyrskjøt is board member at BioXpedia.

Jørgen Bjerggaard Jensen is proctor for Intuitive Surgery, is a member of advisory board for Olympus Europe, Ambu, Cepheid, Janssen, and Ferring and has sponsored research agreements with Medac, Photocure ASA, Cepheid, Olympus, and Ferring.

Asaf Zviran is the co-founder and a member of the board of directors of C2i Genomics. Boris Oklander is the co-founder and CTO of C2i Genomics.

Santiago Gonzalez, Maja Kuzman, Jurica Levatic, Dunja Glavas, Ryan Ptashkin, James Smadbeck, Danielle Afterman, Tomer Lauterman, Yarin Cohen, Zohar Donenhirsh, Iman Tavassoly, Ury Alon are employees of C2i Genomics. Paz Polak is a former employee of C2i Genomics.

Figure legends

Fig. 1: Study design and analysis scheme

a, the study design showing scheduled CT scanning (thorax- abdomen) and clinical sample collection. To exclude distant metastasis full body PET/CT scans were performed after diagnosis. Plasma samples up to 12-months post RC were analyzed in this study. **b**, patient specific signature analysis. WGS of tumor/germline pairs followed by genome-wide integration of somatic mutations, structural variation and copy number alterations enriched by signal processing and AI-based error suppression, were used to generate patient-specific tumor signatures (panel 1). The patient-specific tumor signatures were used for determining presence or absence of ctDNA in WGS data from plasma cfDNA (panel 2 and 3). **c**, reproducibility of the method was established through independent processing of the tumor, germline and blood samples at two different laboratories in Denmark and The United States. The comparison included 52 blood samples from 18 patients. Color key, red = detected at both laboratories, black = detected at one of the laboratories and white = tumor fraction below threshold at both laboratories. The coefficient of determination was R^2=0.8 (all samples), and R^2=0.99 (samples detected at both laboratories, red circles).

Fig. 2: Longitudinal ctDNA results for all patients

Horizontal lines represent the disease courses of the patients, and circles represent ctDNA status. Treatment and imaging information are indicated for each patient (see color key). Patients are ordered by decreasing overall survival for patients with and without disease relapse. Patients 4175 and 4250 were not able to undergo RC and time zero for these patients is the scheduled time for surgery.

Fig. 3: ctDNA detection for prognosis assessment

a, association between plasma ctDNA status before NAC and recurrence status within one year after RC including only patients with at least two years of follow-up after RC for non-relapse patients. **b**, Kaplan-Meier survival analysis of RFS and plasma ctDNA status before NAC. **c**, Kaplan-Meier survival analysis of OS and plasma ctDNA status before NAC. **d**, Association between plasma ctDNA status before RC (after NAC) and recurrence status within one year after RC including only patients with at least two years of follow-up after RC for non-relapse patients. **e**, Kaplan-Meier survival analysis of RFS and plasma ctDNA status before RC. **f**, Kaplan-Meier survival analysis of OS and plasma ctDNA status before RC. **g**, Association between accumulated plasma ctDNA status up to the one year post RC visit and recurrence status within 18 months after the last plasma sample was analyzed for ctDNA. Only non-relapse patients with at least 18 months of follow-up after the last plasma sample were included. **h**, Kaplan-Meier survival analysis of RFS and accumulated plasma ctDNA status

after RC. **i**, Kaplan-Meier survival analysis of OS and accumulated plasma ctDNA status after RC. Hazard ratios (HR) and associated 95% confidence intervals (CI) and p-values are displayed on each Kaplan-Meier plot (cox regression analysis). A significant statistical difference between ctDNA status and recurrence was determined using Fisher's exact test.

Fig. 4: ctDNA measurements for detecting disease relapse and treatment response

a, lead time in days between molecular recurrence (ctDNA positivity) and clinical recurrence (radiographic imaging positive). Statistical significance was calculated using paired Wilcoxon Rank test. **b**, Association between ctDNA status before NAC and pathological downstaging. **c**, Association between ctDNA status beforeRC and pathological downstaging. **d**, Association between ctDNA clearance after NAC and pathological downstaging. **e**, association between pathological downstaging and recurrence status within one year after RC for patients who received minimum 3 series of NAC. **f**, Kaplan-Meier survival analysis of RFS and pathological downstaging for patients that have received minimum 3 cycles of NAC. **g**, Association between ctDNA clearance after NAC and recurrence status within one year after RC for patients who received minimum 3 series of NAC. **h**, Kaplan-Meier survival analysis of RFS and ctDNA clearance after NAC for patients who received minimum 3 series of NAC. Hazard ratios (HR) and associated 95% confidence intervals (CI) and p-values are displayed on each Kaplan-Meier plot (cox regression analysis). Significant statistical difference between categorical variables was determined using Fisher's exact test. **i**, tumor fraction (TF) for metastatic lesions divided in 2 groups, lung metastatic sites and all other metastatic sites. **j**, TF stratified by all individual metastatic sites metastatic. Only post RC cfDNA TF were included and only TF>0 was used.

Fig. 5: Genomic characterization of primary tumors

a, Genomic landscape of 112 primary tumors showing the mutational load including the number of single-nucleotide variants and indels, alterations in bladder cancer driver genes having a mutation frequency above 10% in the cohort, whole-genome doubling (WGD) status, contribution of single base substitution (SBS) signatures, contribution of small insertions and deletions (ID) signatures and clinical variables. Asterisks indicate genes significantly mutated in the cohort as defined by the dndscv algorithm. **b,** Number of mutations in the SBS92 context according to smoking status of the patients. **c,** Number of mutations in the SBS92 context versus the number of smoking pack years for current and former smokers. **d,** Number of small insertions and deletions in the ID3 context according to smoking status of the patients. **e,** Number of small insertions and deletions in the ID3 context versus the number of smoking pack years for current and former smokers. **f,** Association between pathological response to

neoadjuvant chemotherapy (NAC) and the combination of *ERCC2* mutational status and SBS5 contribution (above or below the median SBS5 contribution).

Fig. 6: Genomic evolution of bladder cancer delineated by ctDNA analysis
a, Relative contribution of fitted bladder signatures in plasma samples with a tumor fraction above 10% per patient. Each patient is represented by 3 bars which are the signature activity corresponding to: (left) mutations present only in the primary tumor, (right) mutations present exclusively in the ctDNA, and (middle) mutations present both in primary tumor and ctDNA. **b,** Same representation of the bladder mutational signatures but normalizing by the total number of SNVs per sample. **c,** The percentage of the genome that has changed its copy number compared with the initial primary tumor sample for all plasma samples with a tumor fraction above 10%. **d,** Examples of changes in copy numbers comparing primary (top row) versus ctDNA (following rows) for patient 4105 and 5113.

References

1. Heitzer, E., Auinger, L. & Speicher, M. R. Cell-Free DNA and Apoptosis: How Dead Cells Inform About the Living. *Trends Mol. Med.* **26**, 519–528 (2020).
2. Cherepanova, A. V., Tamkovich, S. N., Bryzgunova, O. E., Vlassov, V. V. & Laktionov, P. P. Deoxyribonuclease activity and circulating DNA concentration in blood plasma of patients with prostate tumors. *Ann. N. Y. Acad. Sci.* **1137**, 218–221 (2008).
3. Tamkovich, S. N. *et al.* Circulating DNA and DNase activity in human blood. *Ann. N. Y. Acad. Sci.* **1075**, 191–196 (2006).
4. Yu, S. C. Y. *et al.* High-resolution profiling of fetal DNA clearance from maternal plasma by massively parallel sequencing. *Clin. Chem.* **59**, 1228–1237 (2013).
5. Khier, S. & Gahan, P. B. Hepatic Clearance of Cell-Free DNA: Possible Impact on Early Metastasis Diagnosis. *Mol. Diagn. Ther.* **25**, 677–682 (2021).
6. Khier, S. & Lohan, L. Kinetics of circulating cell-free DNA for biomedical applications: critical appraisal of the literature. *Future Sci OA* **4**, FSO295 (2018).
7. Reinert, T. *et al.* Analysis of Plasma Cell-Free DNA by Ultradeep Sequencing in Patients With Stages I to III Colorectal Cancer. *JAMA Oncol* (2019) doi:10.1001/jamaoncol.2019.0528.

8. Abbosh, C. *et al.* Phylogenetic ctDNA analysis depicts early-stage lung cancer evolution. *Nature* **545**, 446–451 (2017).
9. Christensen, E. *et al.* Early Detection of Metastatic Relapse and Monitoring of Therapeutic Efficacy by Ultra-Deep Sequencing of Plasma Cell-Free DNA in Patients With Urothelial Bladder Carcinoma. *J. Clin. Oncol.* JCO1802052 (2019).
10. Sung, H. *et al.* Global Cancer Statistics 2020: GLOBOCAN Estimates of Incidence and Mortality Worldwide for 36 Cancers in 185 Countries. *CA Cancer J. Clin.* **71**, 209–249 (2021).
11. Witjes, J. A. *et al.* European Association of Urology Guidelines on Muscle-invasive and Metastatic Bladder Cancer: Summary of the 2020 Guidelines. *Eur. Urol.* **79**, 82–104 (2021).
12. Powles, T. *et al.* ctDNA guiding adjuvant immunotherapy in urothelial carcinoma. *Nature* **595**, 432–437 (2021).
13. van Dorp, J. *et al.* High- or low-dose preoperative ipilimumab plus nivolumab in stage III urothelial cancer: the phase 1B NABUCCO trial. *Nat. Med.* (2023) doi:10.1038/s41591-022-02199-y.
14. Moser, T., Kühberger, S., Lazzeri, I., Vlachos, G. & Heitzer, E. Bridging biological cfDNA features and machine learning approaches. *Trends Genet.* (2023) doi:10.1016/j.tig.2023.01.004.
15. Zviran, A. *et al.* Genome-wide cell-free DNA mutational integration enables ultra-sensitive cancer monitoring. *Nat. Med.* **26**, 1114–1124 (2020).
16. Widman, A. J. *et al.* Machine learning guided signal enrichment for ultrasensitive plasma tumor burden monitoring. *bioRxiv* 2022.01.17.476508 (2022) doi:10.1101/2022.01.17.476508.
17. Herberts, C. *et al.* Deep whole-genome ctDNA chronology of treatment-resistant prostate cancer. *Nature* **608**, 199–208 (2022).
18. Martínez-Jiménez, F. *et al.* A compendium of mutational cancer driver genes. *Nat. Rev. Cancer* **20**, 555–572 (2020).

19. Martincorena, I. *et al.* Universal Patterns of Selection in Cancer and Somatic Tissues. *Cell* **171**, 1029–1041.e21 (2017).
20. Gerstung, M. *et al.* The evolutionary history of 2,658 cancers. *Nature* **578**, 122–128 (2020).
21. Gonzalez, S., Lopez-Bigas, N. & Gonzalez-Perez, A. Copy number footprints of platinum-based anticancer therapies. *PLoS Genet.* **19**, e1010634 (2023).
22. Bielski, C. M. *et al.* Genome doubling shapes the evolution and prognosis of advanced cancers. *Nat. Genet.* **50**, 1189–1195 (2018).
23. Lawson, A. R. J. *et al.* Extensive heterogeneity in somatic mutation and selection in the human bladder. *Science* **370**, 75–82 (2020).
24. Islam, S. M. A. *et al.* Uncovering novel mutational signatures by de novo extraction with SigProfilerExtractor. *Cell Genom* **2**, None (2022).
25. Alexandrov, L. B. *et al.* The repertoire of mutational signatures in human cancer. *Nature* **578**, 94–101 (2020).
26. Tate, J. G. *et al.* COSMIC: the Catalogue Of Somatic Mutations In Cancer. *Nucleic Acids Res.* **47**, D941–D947 (2019).
27. Degasperi, A. *et al.* A practical framework and online tool for mutational signature analyses show inter-tissue variation and driver dependencies. *Nat Cancer* **1**, 249–263 (2020).
28. Polak, P. *et al.* Reduced local mutation density in regulatory DNA of cancer genomes is linked to DNA repair. *Nat. Biotechnol.* **32**, 71–75 (2014).
29. Haradhvala, N. J. *et al.* Mutational Strand Asymmetries in Cancer Genomes Reveal Mechanisms of DNA Damage and Repair. *Cell* **164**, 538–549 (2016).
30. Kim, J. *et al.* Somatic ERCC2 mutations are associated with a distinct genomic signature in urothelial tumors. *Nat. Genet.* **48**, 600–606 (2016).
31. Adalsteinsson, V. A. *et al.* Scalable whole-exome sequencing of cell-free DNA reveals high concordance with metastatic tumors. *Nat. Commun.* **8**, 1324 (2017).
32. Parikh, A. R. *et al.* Liquid versus tissue biopsy for detecting acquired resistance and

tumor heterogeneity in gastrointestinal cancers. *Nat. Med.* **25**, 1415–1421 (2019).

33. Balbás-Martínez, C. *et al.* Recurrent inactivation of STAG2 in bladder cancer is not associated with aneuploidy. *Nat. Genet.* **45**, 1464–1469 (2013).
34. Robertson, A. G. *et al.* Comprehensive Molecular Characterization of Muscle-Invasive Bladder Cancer. *Cell* **171**, 540–556.e25 (2017).
35. Patel, K. M. *et al.* Association Of Plasma And Urinary Mutant DNA With Clinical Outcomes In Muscle Invasive Bladder Cancer. *Sci. Rep.* **7**, 5554 (2017).
36. Vandekerkhove, G. *et al.* Plasma ctDNA is a tumor tissue surrogate and enables clinical-genomic stratification of metastatic bladder cancer. *Nat. Commun.* **12**, 184 (2021).
37. Treatment Of Metastatic Bladder Cancer at the Time Of Biochemical reLApse Following Radical Cystectomy - Full Text View - ClinicalTrials.gov. https://clinicaltrials.gov/ct2/show/NCT04138628.
38. A Study of Atezolizumab Versus Placebo as Adjuvant Therapy in Patients With High-Risk Muscle-Invasive Bladder Cancer Who Are ctDNA Positive Following Cystectomy - Full Text View - ClinicalTrials.gov. https://clinicaltrials.gov/ct2/show/NCT04660344.
39. Bando, H. *et al.* Effects of Metastatic Sites on Circulating Tumor DNA in Patients With Metastatic Colorectal Cancer. *JCO Precis Oncol* **6**, e2100535 (2022).
40. Frankell, A. M. *et al.* The evolution of lung cancer and impact of subclonal selection in TRACERx. *Nature* **616**, 525–533 (2023).
41. Abbosh, C. *et al.* Tracking early lung cancer metastatic dissemination in TRACERx using ctDNA. *Nature* **616**, 553–562 (2023).
42. Loriot, Y. *et al.* Erdafitinib in Locally Advanced or Metastatic Urothelial Carcinoma. *N. Engl. J. Med.* **381**, 338–348 (2019).
43. Harris, P. A. *et al.* A metadata-driven methodology and workflow process for providing translational research informatics support. *J. Biomed. Inform.* **42**, 377–381 (2009).
44. Harris, P. A. *et al.* The REDCap consortium: Building an international community of software platform partners. *J. Biomed. Inform.* **95**, 103208 (2019).

45. Birkenkamp-Demtröder, K. *et al.* Genomic Alterations in Liquid Biopsies from Patients with Bladder Cancer. *Eur. Urol.* **70**, 75–82 (2016).
46. Lee, S. *et al.* NGSCheckMate: software for validating sample identity in next-generation sequencing studies within and across data types. *Nucleic Acids Res.* **45**, e103 (2017).
47. Jiang, H., Lei, R., Ding, S.-W. & Zhu, S. Skewer: a fast and accurate adapter trimmer for next-generation sequencing paired-end reads. *BMC Bioinformatics* **15**, 182 (2014).
48. van der Auwera, G. & O'Connor, B. D. *Genomics in the Cloud: Using Docker, GATK, and WDL in Terra*. (O'Reilly Media, Incorporated, 2020).
49. Kim, S. *et al.* Strelka2: fast and accurate calling of germline and somatic variants. *Nat. Methods* **15**, 591–594 (2018).
50. Shen, R. & Seshan, V. E. FACETS: allele-specific copy number and clonal heterogeneity analysis tool for high-throughput DNA sequencing. *Nucleic Acids Res.* **44**, e131 (2016).
51. Danecek, P. *et al.* Twelve years of SAMtools and BCFtools. *Gigascience* **10**, (2021).
52. International HapMap Consortium. The International HapMap Project. *Nature* **426**, 789–796 (2003).
53. McLaren, W. *et al.* The Ensembl Variant Effect Predictor. *Genome Biol.* **17**, 122 (2016).
54. Tamborero, D. *et al.* Cancer Genome Interpreter annotates the biological and clinical relevance of tumor alterations. *Genome Med.* **10**, 25 (2018).
55. Wagner, A. H. *et al.* A harmonized meta-knowledgebase of clinical interpretations of somatic genomic variants in cancer. *Nat. Genet.* **52**, 448–457 (2020).
56. Priestley, P. *et al.* Pan-cancer whole-genome analyses of metastatic solid tumours. *Nature* **575**, 210–216 (2019).

a

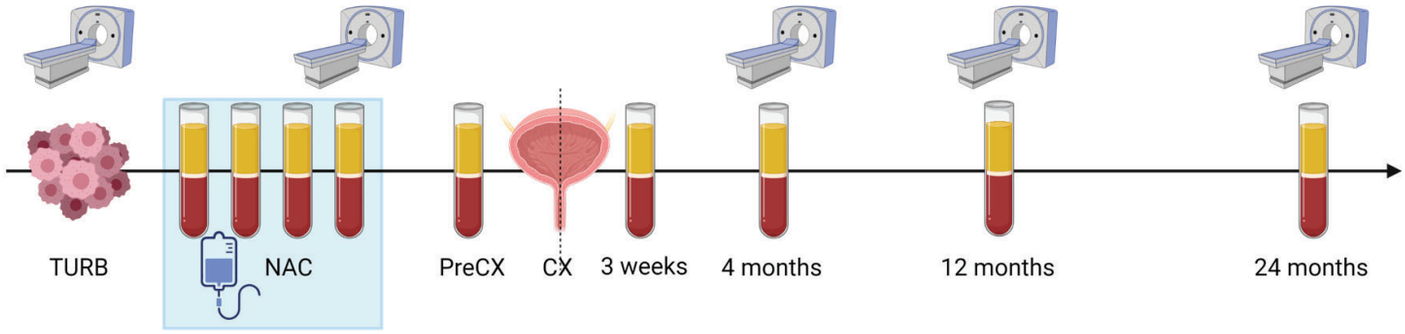

b

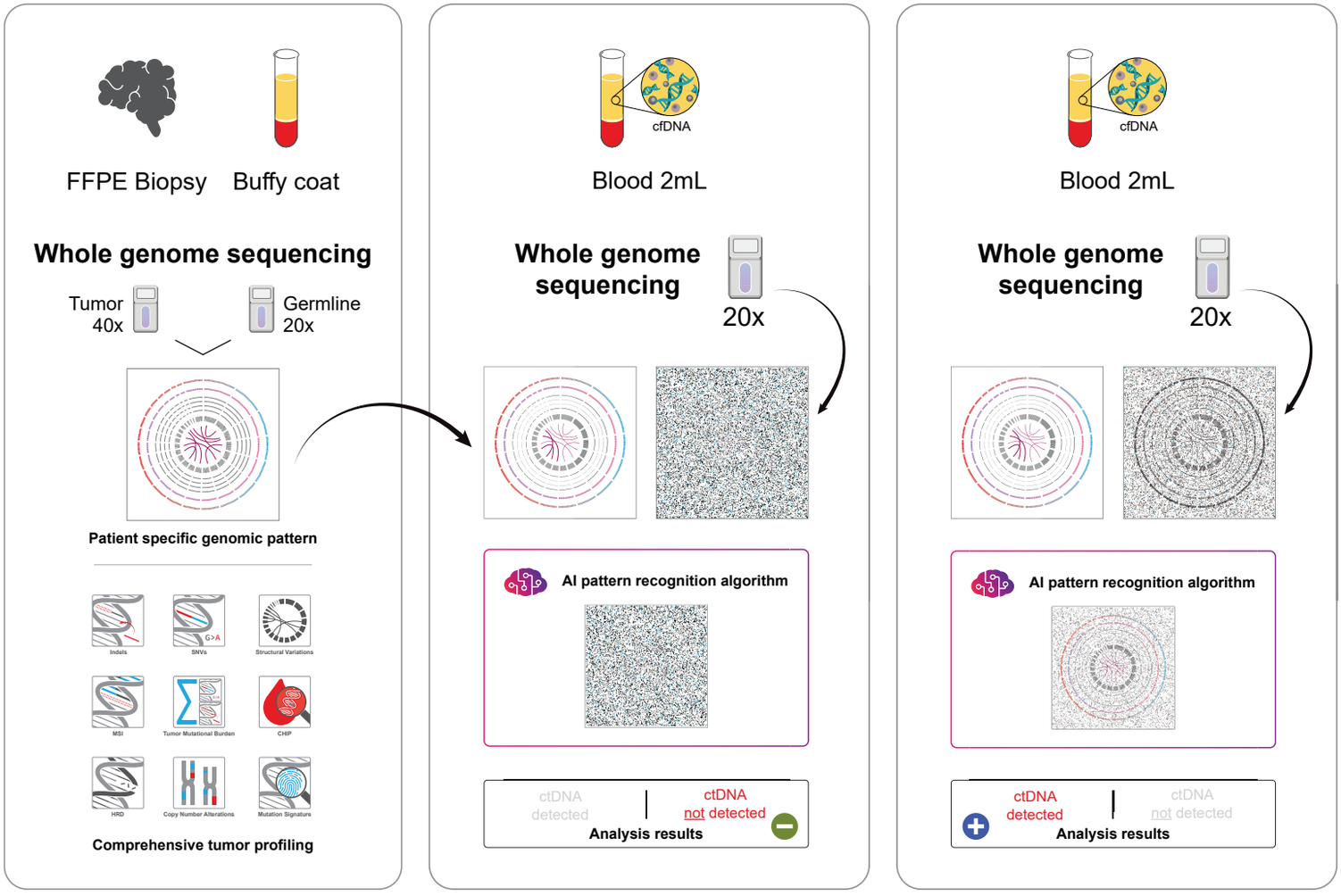

c